

Enriched fracture mechanics from discrete elements method

E. Morice¹, S. Pommier¹ and A. Delaplace^{1,2}

¹ LMT-Cachan (ENS Cachan/CNRS/UPMC/PRES UniverSud Paris)

61, avenue du Président Wilson 94235 Cachan

² Lafarge Centre de Recherche -- Mécanique et Modes Constructifs

95 rue du Montmurier – 38291 Saint Quentin Fallavier

ABSTRACT. *Crack growth in non-linear quasi-brittle materials is addressed by a new approach. This approach is consistent with the Linear Elastic Fracture Mechanics Framework; the velocity field around the crack tip is represented by a sum of terms, each term being defined as the product of a shape function and an intensity factor. So as to enrich the LEFM kinematics, additional shape functions are introduced to account for the non-linear behaviour of the material. To do so, the discrete element method is used to compute the velocity field around a crack tip for nominal stress intensity factors histories, using boundary conditions extracted from finite element calculations. Preliminary analyses are executed to construct a basis of shape functions for mode I and mode II, including linear and non-linear terms, using a proper orthogonal decomposition. Once this is done, the velocity field computed using the discrete element method for various mixed mode loading schemes can be projected onto this basis of shape functions, which allows condensing the evolution of the damage field around the crack tip into the evolution law of the “non-linear” intensity factors associated with each mode.*

INTRODUCTION

Being able to accurately predict the leakage rate through a cracked or damaged concrete shell remains a major challenge to nuclear safety. It requires accounting explicitly for opening and growth of through thickness cracks. The linear elastic fracture mechanics framework should be the best suited for this type of problems. However the underlying assumption of linear elasticity makes it inappropriate to model the permeability of concrete shells.

As a matter of fact, quasi-brittle materials such as mortar, concrete or rocks display a non-linear quasi-brittle behaviour. The crack tip process zone consists in a high number of micro-cracks, among which some coalesce to promote macroscopic crack growth while others, that remain unconnected with the macro-crack, produce a shielding effect to the macro-crack and an overall non-linear behaviour of the cracked structure.

The discrete element method (DEM) is attractive to deal with problems involving damage and micro-cracking in heterogeneous quasi-brittle materials. The material is modelled as a Voronoi tessellation of particles and a set of connections between them, modelled as cohesive forces. The maximum allowable strain in each connection is statistically distributed so as to represent the heterogeneity of the material. The process of micro-cracking is then described by the breaking of connections between particles

and generates naturally the appropriate complexity (damage localization, cracks pattern formation, etc.).

Nevertheless, modelling the behavior of a nuclear core concrete shell by the DEM remains up to now out of reach. The aim of this study is thus to enrich the kinematics of the crack tip region by adding additional fields stemming from DEM simulations. As in LEFM, these fields are expressed as the product of an intensity factor, handled as a degree of freedom, and of a shape function defined *a priori* and characterizing the geometry of the velocity field in the process zone. In I+II mixed mode conditions, the evolutions of 4 intensity factors, a linear and a non-linear ones for each mode, thus fully characterize the kinematics of the crack tip region. The discrete element method is used to compute velocity field evolutions for various mixed mode loading histories, which are then post-treated so as to reduce them into evolutions of four intensity factors.

DISCRETE MODEL

In the considered discrete model ([1]), the material is described as a Voronoï particle assembly, representative of the material heterogeneity (Fig. 1(a)). Basically two types of interactions are considered, cohesive forces and contact forces, however our study focuses only on tension loading, so we'll consider only cohesive forces.

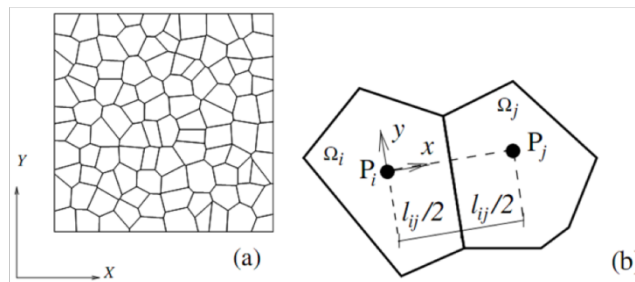


Figure 1. Discrete model (a) and representation of Voronoï cells and their connections (b).

Each particle possess 3 degrees of freedom (2 in translations and 1 in rotation), and the interaction between two particles is represented by a 6 x 6 local stiffness matrix. Following Schlangen and Garboczi ([4]), Van Mier et al. ([5]), an Euler-Bernoulli beam matrix is used in the model to connect each pair of neighboring particles i and j (Fig. 1(b)).

Considering an ideally elastic-brittle behavior for the beams renders damage evolution. The breaking criterion for a connection l_{ij} between two particles i and j , is function of the strain of the beam ε used as a connector and of the rotation values θ_i and θ_j of particles i and j :

$$P_{ij} = \left(\frac{\varepsilon_{ij}}{\varepsilon_{cr}} \right)^2 + \left(\frac{\max(|\theta_i|, |\theta_j|)}{\theta_{cr}} \right)^2 \geq 1 \quad (1)$$

ε_{cr} and θ_{cr} are two material parameters, the first one controlling essentially the tensile behavior of the discrete model, and the second its compressive behavior. These two parameters are statistically distributed so as to account for the heterogeneity of the material

BOUNDARY CONDITIONS

The model is constructed so as to be driven in nominal stress intensity factor boundary conditions. For this purpose, we use both FE and DEM analyses. In both cases, the region of interest (ROI) is a $12\text{ mm} \times 12\text{ mm}$ square section, having the crack tip in its centre at the beginning of each computation. The first step of the analysis is performed using the finite element method and a linear elastic material behaviour. The FE model is a $5\text{ m} \times 5\text{ m}$ square plate with a centered crack with a length $2a = 100\text{ mm}$, the FE mesh is refined within the ROI around the crack tip. The displacement of the nodes located along the faces of the ROI is extracted from the FE results of simulations with either or and is then assigned as reference boundary conditions for DEM analyses. The discrete element model consists of a $12\text{ mm} \times 12\text{ mm}$ square ROI. The discrete element mesh was constructed so as to display a symmetry plane along the crack plane.

CRACK TIP FIELDS IN MIXED MODE I + II LOADING CONDITIONS

Assumptions

The DEM model can hence be driven in terms of nominal stress intensity factors histories. The velocity field evolutions, computed using the DEM, are then post-treated to extract their main features. For this purpose, the following hypotheses are considered. First, to be consistent with the LEFM framework, the crack is modelled by a local plane and front. This assumption allows defining a local axis system R_T and partitioning the velocity field into modes. The mode I consists of the symmetric part of the velocity field $v(P,t)$ with respect to the local axis system R_T attached to the crack tip and the mode II, to its anti-symmetric part. In addition, with respect to R_T , the geometry of the crack is assumed to remain locally unchanged by changes in the scales, implying that the crack tip fields can be expressed as the product of an angular distribution and of a scale function. The second main hypothesis is thus to approximate each part of the crack tip velocity field as the product of a shape function and of an intensity factor. For each fracture mode, a “linear elastic” shape function is first introduced to be consistent with the LEFM framework. Then an additional shape function is constructed to carry the non-linear behavior of the crack tip process zone induced by the presence of micro-cracks.

Construction of linear elastic shape functions

The linear elastic reference fields u_e^I and u_e^{II} are first obtained from elastic simulations using the discrete model. In order to model a linear elastic response with the discrete element model, the connections between particles are all considered as unbreakable. The linear elastic reference field for each mode is then obtained after partitioning the displacement field computed by DEM analysis into mode I and mode II components.

Construction of additional shape functions

To obtain the two additional fields u_c^I and u_c^{II} , the discrete element model is loaded either in mode I or in mode II. The connections between particles are now allowed to break. The solution $v(P,t)$ of a monotonic loading case is post-treated as follows. First, the DEM velocity field $v(P,t)$ is projected onto the linear elastic reference fields. The projections $\dot{\tilde{K}}_I$ (resp. $\dot{\tilde{K}}_{II}$) of $v(P,t)$ onto u_e^I (resp. u_e^{II}), can slightly differ from the nominal stress intensity factor loading rate \dot{K}_I^∞ (resp. \dot{K}_{II}^∞). As a matter of fact, two types of stresses contribute to the ‘‘LEFM’’ response of the cracked structure, the applied stress field featured by K_I^∞ and the internal stress field that arises from the shielding effect of the field of micro-cracks within the process zone.

$$\dot{\tilde{K}}_I = \frac{\int_{r=0}^{r_{\max}} \int_{\theta=-\pi}^{\pi} v(P,t) \cdot u_e^I(P) r d\theta dr}{\int_{r=0}^{r_{\max}} \int_{\theta=-\pi}^{\pi} u_e^I(P) \cdot u_e^I(P) r d\theta dr} \quad (2)$$

The residue is then calculated as follows:

$$v^{res}(P,t) = v(P,t) - \dot{\tilde{K}}_I(t) u_e^I(P) \quad (3)$$

This residue can then be partitionned using the Karhunen-Loeve transform [3] into a sum of a product of spatial fields, mutually orthogonal, and their intensity factors. We only keep the first term for each mode. Assuming that the two linear elastic reference fields (u_e^I and u_e^{II}) and the two additional fields (u_c^I and u_c^{II}) that were constructed using either linear elastic or non-linear conditions for monotonic mode I or mode II loading phases can be used to represent any complex mixed mode loading scheme, we can then approximate the crack tip velocity field as follows:

$$v(P,t) \approx \tilde{v}(P,t) = \dot{\tilde{K}}_I(t) u_e^I(P) + \dot{\tilde{K}}_{II}(t) u_e^{II}(P) + \dot{\rho}_I(t) u_c^I(P) + \dot{\rho}_{II}(t) u_c^{II}(P) \quad (4)$$

This assumption is valid only if the process zone is constrained inside an elastic bulk that controls and limits the movement inside the process zone. The Karhunen-Loeve transform was selected because it uses the self-correlation matrix of the movement. In other words, it partitions the movement inside the process zone into uncorrelated or independent movements. As a consequence, the intensity factors represent the independent degrees of freedom of the process zone.

With this hypothesis, the evolution of the four intensity factors ($K_I, K_{II}, \rho_I, \rho_{II}$) of the four reference fields ($u_e^I, u_e^{II}, u_c^I, u_c^{II}$) is a condensed measure of the behavior of the process zone. To verify the quality and the suitability of that hypothesis, the error associated to the approximation of the velocity field is calculated at each time step.

Extraction of the intensity factors

Having at our disposal an orthogonal basis of spatial reference fields ($u_e^I, u_e^{II}, u_c^I, u_c^{II}$), defined a priori for a given material, makes it possible to project the velocity field $v(P,t)$, obtained for any loading sequence, onto this basis.

First the rate of the mode I (resp. mode II) linear-elastic intensity factor K_I (resp. K_{II}) is extracted as shown in Eq. 5. This rate is given in $\text{MPa}\sqrt{\text{m}}\cdot\text{s}^{-1}$ and is very close to the rate of the nominal applied stress intensity factor K_I^∞ (resp. K_{II}^∞). We then proceed as follows to extract the rate of the mode I (resp. mode II) non-linear intensity factor ρ_I (resp. ρ_{II}) :

$$\dot{\rho}_I = \frac{\int_{r=0}^{r_{\max}} \int_{\theta=-\pi}^{\pi} v(P,t) \cdot u_c^I(P) r d\theta dr}{\int_{r=0}^{r_{\max}} \int_{\theta=-\pi}^{\pi} u_c^I(P) \cdot u_c^I(P) r d\theta dr} \quad (5)$$

Error calculation

Once the four intensity factors are extracted, an approximation of the computed velocity field $v(P,t)$ is provided in Eq. 4. It is useful to define the errors associated with this approximation:

- the error $C_1(t)$, associated with a linear elastic representation of the velocity field
- the error $C_2(t)$, associated with a non-linear representation of the velocity field.

The error $C_1(t)$ and the relative error $C_{1R}(t)$ are calculated as follows :

$$C_1(t) = \sqrt{\int_D \left(v(P,t) - \tilde{K}_I(t)u_e^I(P) - \tilde{K}_{II}(t)u_e^{II}(P) \right)^2 dv}, \quad C_{1R}(t) = C_1(t) / \sqrt{\int_D (v(P,t))^2 dv} \quad (6)$$

The error $C_2(t)$ and the relative error $C_{2R}(t)$ are calculated as follows :

$$C_2(t) = \sqrt{\int_D (v(P,t) - \tilde{v}(P,t))^2 dv}, \quad C_{2R}(t) = C_2(t) / \sqrt{\int_D (v(P,t))^2 dv} \quad (7)$$

The errors C_2 and C_{2R} indicate when this approach is valid and the difference between C_{1R} and C_{2R} indicates whether or not a non-linear approach is really needed, or in other words, when the process zone behavior can be considered as having a linear-elastic behavior or not.

ADDITIONAL SHAPE FUNCTIONS

R-dependency

To illustrate this method (Fig. 2), the additional fields for each mode, obtained by a proper orthogonal decomposition, were post-treated a second time so as to partition them into a function of the distance to the crack tip r and of the angular location θ . The r -dependency is the same for the two modes and displays an exponential decay.

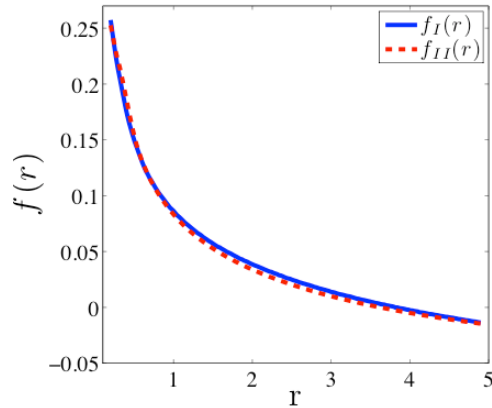


Figure 2: Comparison of r -dependency of mode I and II components.

θ -dependency

The θ -shape functions $g(\theta)$ possess two components (a radial and a hook ones). For the sake of simplicity, it was chosen to represent it using the deformation of an initial circle induced by either the mode I or the mode II θ -shape function, respectively Fig. 3(a) and Fig. 3(b). In both cases, there is a discontinuity of the velocity field along the crack plane, the mode I component being symmetric and the mode II antisymmetric.

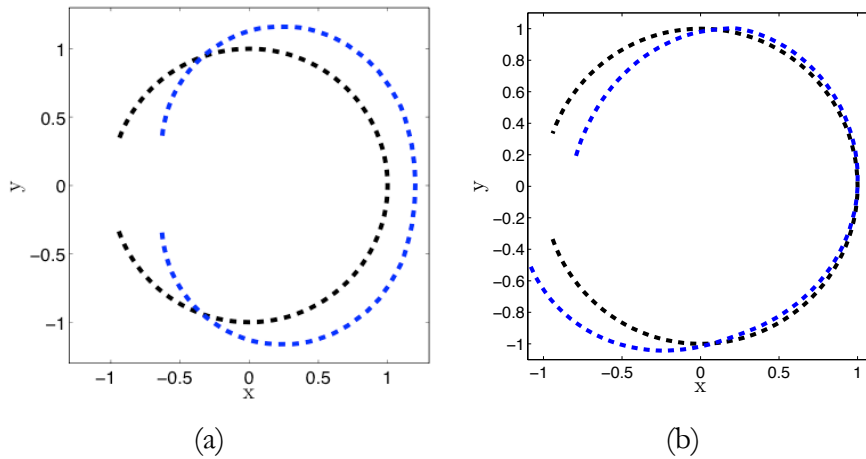


Figure 3: Dependency in θ of the complementary fields in mode I (a) and II (b).

The discontinuity of the opening displacement at the circle ends ($\theta=-\pi$ and $\theta=\pi$) in mode I, analogous to a CTOD, is used to make the mode I additional field dimensionless. In mode II, the sliding displacement discontinuity, analogous to a CTSD, is used to make the mode II additional field dimensionless.

INTENSITY FACTORS

Computations have then been made for mode I and II loading cycles with cyclically increasing amplitudes. For each time increment, the velocity field computed using the discrete element method is projected onto the basis of reference fields that was

constructed using previous calculations. In Fig. 4 (a) and (b), the non-linear intensity factor ρ_I (resp. ρ_{II}) is plotted against the nominal applied stress intensity factor K_I^∞ (resp. K_{II}^∞). It is clear in this graph that ρ_I (resp. ρ_{II}) does not represent directly the damage of the process zone. In fact, ρ_I (resp. ρ_{II}) represent the contribution of micro-cracks to the velocity field in the process zone. When the process zone is loaded or unloaded below the maximum value of K_I^∞ (resp. K_{II}^∞) reached previously, there is no longer break of connections. In this case, we first observe that the $K_I^\infty - \rho_I$ curve is a straight line and that its slope is constant. We also observe that the two errors C_{1R} and C_{2R} are both very small. During such loading and unloading phases existing micro-cracks do cyclically close and open, but there is no creation of new micro-cracks.

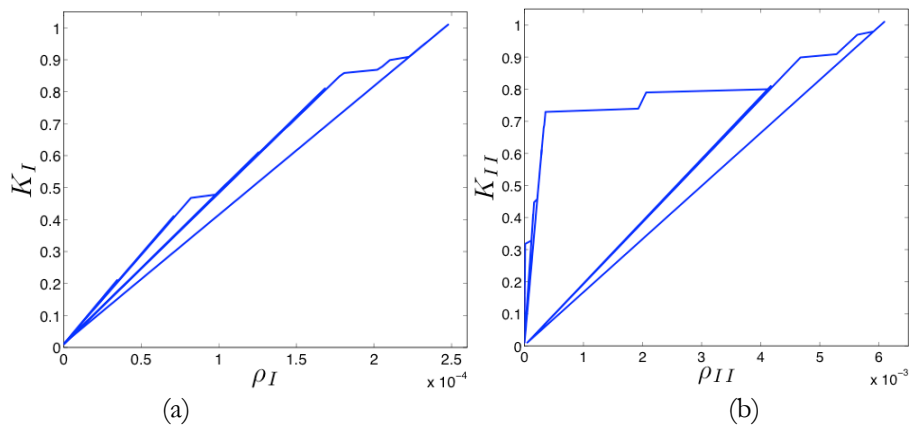


Figure 4: Evolution of non-linear intensity factors with the stress intensity factor in mode I (a), and in mode II (b).

However, when new micro-cracks are created, i.e. when connections are broken, the slope of the $K_I^\infty - \rho_I$ curve changes. In addition, we observe that both C_{1R} and the difference between C_{1R} and C_{2R} increase significantly during loading phases for which connections are broken (in any cases, it is found that C_{2R} is small, well below 0.1%, indicating that the approach is valid).

The damage of the process zone is related to the slope of the $K_I^\infty - \rho_I$ curve during loading phases for which no micro-cracks are created. The evolution law of damage is given by the variation of that slope during loading.

In this first analysis we did not try to load the model above $0.2 \text{ MPa}\cdot\text{m}^{1/2}$, however, we observed that the shielding effect of micro-cracks $\tilde{K}_I K_I^\infty$ is progressively decreasing when the micro-cracks density is increasing.

Loadings sequences at different mode mixity were simulated using the discrete elements model. The evolutions of the intensity factors are shown in Fig.5. Although loading directions were clearly different in terms of K_I^∞ and K_{II}^∞ as shown in Fig. 5(a), it appears there are only two main flow direction in terms of (ρ_I, ρ_{II}) (Fig. 5(b)).

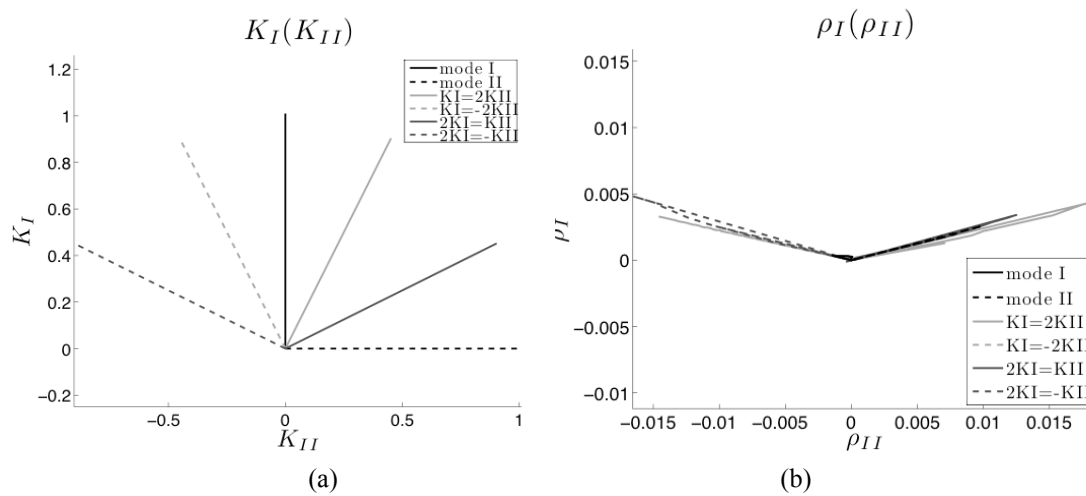


Figure 5: Loading directions in K_I^∞ and K_{II}^∞ diagram for different mode mixity factors (a) and evolutions of complementary intensity factors corresponding (b).

CONCLUSIONS

An enriched kinematic is proposed to feature the crack tip velocity field in quasi-brittle materials. A basis of reference fields was constructed once and for all for a given material. It contains a linear-elastic and non-linear field for each mode. During mixed-mode loading schemes, the velocity field in the process zone computed using the discrete element method, is projected onto this basis so as to extract their intensity factors. The behavior of the crack tip region can then be analyzed through the evolution of the four intensity factors of the four reference fields. For each mode, the intensity factor of the elastic-linear reference field is extremely close to the nominal applied stress intensity factor. The intensity factors of the non-linear reference fields represent the overall contribution of micro-cracks in the process zone to the velocity field for each mode. Evolution laws can be generated using the DEM, that will be used to construct a non-linear constitutive model for the crack tip process zone.

REFERENCES

- [1] Delaplace A., Tensile damage response from discrete element virtual testing, *Geomech. Geoengng.*, 4 (2009) 1, 79-89.
- [2] Pommier S., Hamam R., Incremental model for fatigue crack growth based on a displacement partitioning hypothesis of mode I elastic-plastic displacement fields, *Fatigue Fract. Engng Mater. Struct.*, 30, (2007) 7, 582-598.
- [3] Karhunen K., Über lineare methoden in der wahrscheinlichkeitsrechnung, *Mat.-Phys.*, 37 (1947), 1-79.
- [4] Schlangen E., Garboczi E. J., Fracture simulations of concrete using lattice models: Computational aspects, *Eng. Fract. Mech.*, 57(1997), 319-332.
- [5] Van Mier J. G. M., Van Vlietn M. R. A., Wang T K, Fracture mechanisms in particle composites: statistical aspects in lattice type analysis, *Mech. Mater.*, 34 (2002), 705-724.